Journal of Thermal Analysis and Calorimetry, Vol. 72 (2003) 769–776

CHARACTERISATION OF THE OXIDATION PRODUCTS OF PYRITE BY THERMOGRAVIMETRIC AND EVOLVED GAS ANALYSIS

P. S. Thomas[*]*, D. Hirschausen, R. E. White, J. P. Guerbois and A. S. Ray*

Department of Chemistry, Materials and Forensic Sciences, University of Technology, Sydney, Australia

Abstract

Museum specimens of pyrite are known to undergo oxidation even during storage. Characterisation of the oxidation products is however not always simple due to amorphous character and varying degrees of hydration of the oxidation products. This paper presents an alternative approach to the characterisation of oxidation products by identifying their presence from their characteristic thermal decomposition processes using thermogravimetric and evolved gas analysis. Four pyrite specimens were characterised with varying degrees of oxidation. Iron(II) and iron(III) sulphates were also characterised for comparative purposes. The degradation products were observed to correlate well with the presence of iron(II) sulphate even though there was found to be some discrepancy in the higher temperature decomposition reactions.

Keywords: evolved gas analysis, iron sulphate, pyrite, thermogravimetric analysis

Introduction

Bulk samples of the mineral pyrite (iron disulfide, FeS_2) oxidise unpredictably, resulting in the destruction of valuable museum specimens and geological records [1]. Although considerable research effort has been expended on the mechanisms of pyrite oxidation, or pyrite 'disease', the factors involved in the initiation of sudden, rapid oxidation of bulk specimens are poorly understood. Pyrite is known to be oxidised by atmospheric oxygen and ferric ions [2], and that this process is accelerated by the presence of moisture [3]. The rate and the products of oxidation, and, therefore, the mechanisms, are also a strong function of the relative humidity and the partial pressure of oxygen [4]. Since oxidation is initiated at crystal surfaces, fine grained specimens with a large surface area tend to be more susceptible to degradation than single crystal specimens. These generalisations, however, do not account for the sudden and catastrophic degradation of many bulk pyrite samples which may have been stored carefully.

* Author for correspondence: E-mail: paul.thomas@uts.edu.au

1388–6150/2003/ $ 20.00
© 2003 Akadémiai Kiadó, Budapest
Akadémiai Kiadó, Budapest
Kluwer Academic Publishers, Dordrecht

Characterisation of the oxidation products is also difficult. Due to the interfacial and heterogeneous nature of the oxidation process, oxidation products tend to be nanocrystalline or amorphous and are therefore not easily characterised by traditional techniques such as X-ray diffraction. In this paper the characterisation of the oxidation products by thermogravimetric analysis (TG) coupled with evolved gas analysis using mass spectroscopy (MS) is presented.

Experimental

Unaffected pyrite specimens and specimens showing signs of oxidation were supplied by the Australian Museum, Sydney, and are listed in Table 1. The samples were confirmed to be pyrite by X-ray analysis using a Siemens D5000 diffractometer with CuK_α radiation, although no oxidation products were observed in the degraded specimens. Specimen P1 differed from the other specimens in that P1 contained a significant proportion of quartz (approximately 25% as determined from the mass loss associated with the pyrite to pyrrhotite decomposition at 640°C (Fig. 1)). The 'as received' specimens were crushed by an agate pestle and mortar to produce a powder which was then characterised by TG. As the oxidation process produces hydrated sulphates as the products, iron(II) sulphate heptahydrate ($FeSO_4 \cdot 7H_2O$, ACS Reagent (99+%), Aldrich) and ferric sulphate hydrate ($Fe_2(SO_4)_3 \cdot xH_2O$ (97+%), Aldrich) were also characterised in their 'as received' state.

Table 1 Classification of the pyrite specimens

Specimen	Origin	Description
P1	Kristineberg Mine, Vosterbotten County, Sweden	Undegraded pyrite crystals in quartz
P2	Sepik River, Papua New Guinea	Undergraded pyrite crystals
P3	Huanzala, Peru	Pyrite Dollar showing signs of pyrite disease
P4	Pannawonika, Western Australia	Pyrite nodules extracted from shale, showing significant signs of pyrite disease

TG characterisation was carried out in a Setaram Setsys 16/18 TG-DSC fitted with a capillary in order to sample the volatiles produced during decomposition reactions. The capillary at the base of the TG furnace carried the evolved gases to a Balzers MS for mass analysis. Temperature calibration on the TG was carried out with indium, tin, zinc, antimony, gold and silver. The TG experiments were carried out on 10 to 15 mg specimens in an argon (BOC, high purity, <10 ppm oxygen) atmosphere with a flow rate of 20 cm^3 min^{-1}. Baseline calibrations were also carried out using the same conditions in order to compensate for buoyancy effects. The gas analysis was carried out on the Channel Tron electron multiplier detector of the MS in order to maximise sensitivity. As this detector is not linear, quantitative analysis using

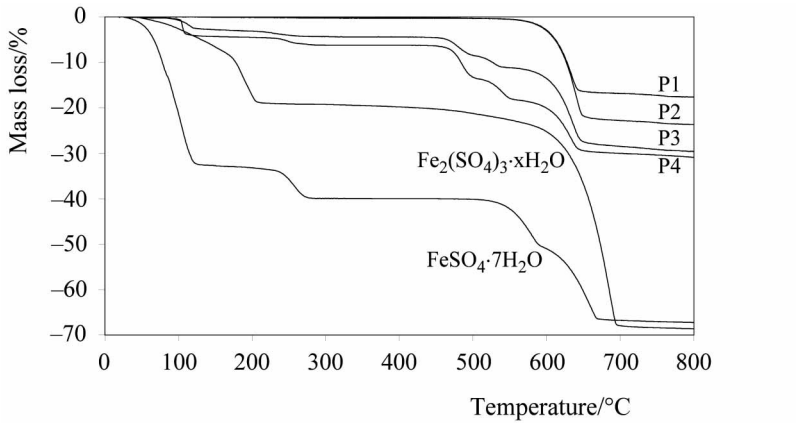

Fig. 1 TG curves for the pyrite and iron sulphate specimens characterised

the MS signal was not possible. The MS data was, therefore, normalised for presentation purposes.

Results and discussion

The mass loss (TG) and differential TG (DTG) curves for samples of undegraded pyrite (P1 and P2) and specimens of pyrite exhibiting signs of decay (P3 and P4) are shown in Figs 1 and 2, respectively. Also included in these figures are the decomposition curves of the iron(II) and iron(III) sulphates. These latter experiments were carried out for comparative purposes aiding the identification of the oxidation products in specimens of pyrite. Significant differences are observed in the decomposition processes of Specimens P1 to P4 and the iron(II) and iron(III) sulphates. The mass losses for each step in the TG curves (in % based on the original mass) are listed in Table 2 and the DTG peaks for each step are listed in Table 3.

Table 2 Mass loss (% based on initial mass) measurements for the decomposition steps observed

Sample	Step 1	Step 2	Step 3	Step 4	Step 5
Reaction mechanism	Eq. (3)	Eq. (4)	Eq. (5)	Eq. (6)	Eq. (1)
P1					17.6
P2					23.7
P3	1.8	0.6	2.8	1.4	17.8
P4	3.0	1.4	4.4	2.5	17.0
$FeSO_4 \cdot 7H_2O$	32.9	7.1	11.3	15.4	
$Fe_2(SO_4)_3 \cdot xH_2O$		19.2[1]		48.9[2]	

[1]Dehydration of iron(III) sulphate hydrate occurs according to: $Fe_2(SO_4)_3 \cdot xH_2O \rightarrow Fe_2(SO_4)_3 + xH_2O$
[2]Thermal decomposition of iron(III) sulphate occurs in accordance with Eq. (2)

Table 3 DTG peak temperatures (°C) for the decomposition steps listed in Table 2

Sample	Step 1	Step 2	Step 3	Step 4	Step 5
P1					633
P2					640
P3	105	233	484	521	631
P4	116	232	481	529	636
$FeSO_4 \cdot 7H_2O$	106	227	580	659	
$Fe_2(SO_4)_3 \cdot xH_2O$		192		686	

The pyrite specimens that had remained unaffected by pyrite disease in storage (P1 and P2) exhibited only a single decomposition DTG peak around 637°C. The mass loss at this decomposition step for the P2 specimen was observed to correspond to the formation of pyrrhotite of composition $Fe_{10}S_{11}$:

$$FeS_2 \rightarrow FeS_{(2-x)} + xS \quad (1)$$

as has been observed elsewhere [5]. This transformation was confirmed by X-ray diffraction analysis of the residue after the heating program had been completed. Only MS peaks at the single decomposition temperature characteristic of the evolution of sulphur were observed. Specimen P1 also decomposed in a similar manner to P2; however, due to the presence of quartz in the matrix the observed mass loss is diminished.

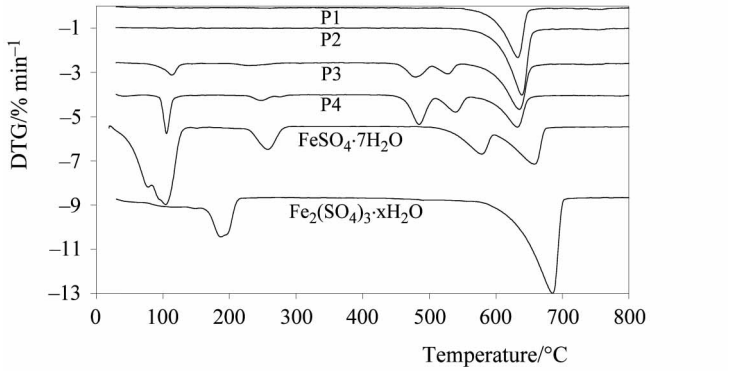

Fig. 2 DTG curves for the pyrite and iron sulphate specimens characterised

The samples which were observed to have suffered pyrite disease produced a number of mass loss steps during the thermal decomposition (Fig. 1). DTG peaks (Fig. 2) were observed around 110 and 250°C, corresponding to the evolution of water, as observed in the MS data; 490 and 530°C corresponding to sulphate decomposition and 635°C which is ascribed to pyrite decomposition. The last three assignments are based on the MS data shown in Figs 3 and 4. 32 ($^{16}O_2^+$ and $^{32}S^+$ ions) and 34 ($^{34}S^+$) atomic mass units (amu) curves are used to differentiate between the presence of sul-

phur and oxygen, and 64 amu to identify the presence of SO_2^+ ion. A single peak is observed in each curve in Fig. 3 corresponding to sulphur evolution in the decomposition of pyrite in the manner of Eq. (3). The presence of oxygen in the argon, even though its concentration is less than 10 ppm, allows oxidation of the sulphur and thus a peak at 64 amu is observed. Figure 4 shows the same set of curves for the partially degraded specimen P4. In this case a number of supplementary peaks are observed. 64 and 32 amu curves show peaks in the range 450 to 550°C. These peaks are not observed in the 34 amu curve. The absence of a peak in the 34 amu curve, coupled with their presence in the 32 amu curve, indicates that the thermal decomposition of the products of pyrite disease yields both SO_2 and O_2. It should be noted that, although not shown in Figs 3 or 4, SO_3 was not observed as a product as no peak was observed in the 80 amu data.

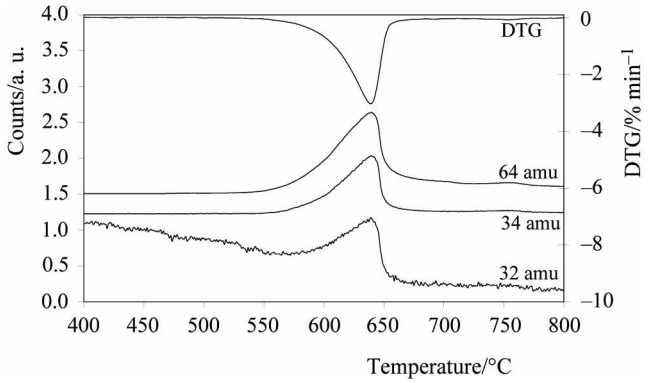

Fig. 3 DTG and MS curves for the thermal decomposition of P2

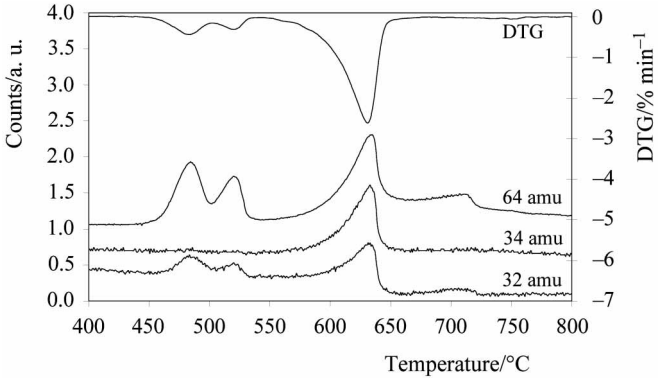

Fig. 4 DTG and MS curves for the thermal decomposition of P4

The process of decomposition of the iron(III) sulphate with a maximum rate at 686°C corresponds to the formation of iron(III) oxide with the evolution of SO_3 as the evolved product and corresponds to the mechanism reported by Paulik *et al*. [6].

$$Fe_2(SO_4)_3 \rightarrow Fe_2O_3 + 3SO_3 \quad (2)$$

The iron(III) sulphate hydrate also has a dehydration peak around 190°C. This peak does not correspond well with the decomposition temperatures of the partially oxidised pyrite specimens. It is evident that the iron(III) sulphate is not a major product of the pyrite decay process even though in aqueous environments it has been shown to be important in catalysing the oxidation process [2].

The thermal decomposition of iron(II) sulphate heptahydrate is observed to be a four-step process. The first step ranging from 50 to 110°C corresponds to the removal of six waters of crystallisation according to:

$$FeSO_4 \cdot 7H_2O \rightarrow FeSO_4 \cdot H_2O + 6H_2O \quad (3)$$

Three overlapping peaks are observed indicating that at least three dehydration sub-steps are involved in this process. The mass loss for this step, however, corresponds to the loss of only 5 water molecules (Table 2). As the higher hydrates are fairly unstable [7] and the sample was observed to dry under the dry flowing argon purge, this reduced water content is not unexpected.

The mass loss at 227°C corresponds well to the removal of a single water molecule:

$$FeSO_4 \cdot H_2O \rightarrow FeSO_4 + H_2O \quad (4)$$

Further heating results in the decomposition of the sulphate which is generally observed to be a two-step process irrespective of the gas environment [7, 8]. A number of mechanisms have been proposed for the two-steps including the formation of hydroxides, mixed valence oxides and oxide sulphates [7, 8]. The decomposition mechanism is however dependent on the purge gas environment. The MS data, using 80 amu SO_3^+ ion, for this decomposition process indicated that no SO_3 was produced. The MS curves for the 64, 34 and 32 amu ions are shown in Fig. 5. The 64 and 34 amu peaks are observed to follow the DTG peaks indicating the evolution of SO_2 during both steps of the decomposition. The 32 amu curve only shows a peak for the higher temperature step indicating that in addition to the production of SO_2, O_2 is also a product. The final product of the decomposition, as determined from X-ray diffrac-

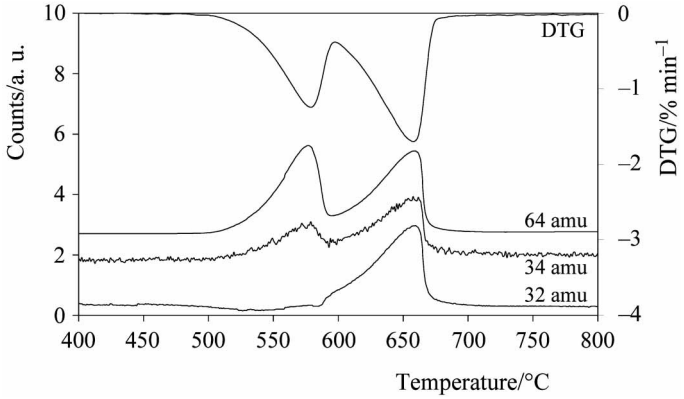

Fig. 5 DTG and MS curves for the thermal decomposition of iron(II) sulphate

tion, was iron(III) oxide which is in agreement with the literature [7, 8]. As this decomposition is carried out in an argon atmosphere, the decomposition process is likely to be:

$$2FeSO_4 \rightarrow Fe_2O_2SO_4 + SO_2 \quad (5)$$

$$Fe_2O_2SO_4 \rightarrow Fe_2O_3 + SO_2 + \tfrac{1}{2}O_2 \quad (6)$$

giving an overall equation for the decomposition as:

$$2FeSO_4 \rightarrow Fe_2O_3 + 2SO_2 + 1/2O_2 \quad (7)$$

The mass loss data confirms the stoichiometry for each of these steps.

A significant difference is, however, observed in the DTG peak positions for these decomposition reactions relative to the decomposition of the partially degraded pyrite specimens. Experimental conditions are known to have a significant effect on the temperature and rate of reactions which has also been observed in the decomposition of iron(II) sulphate [7]. It is, therefore, not surprising that a crystalline and chemically pure bulk specimen of iron(II) sulphate decomposes at higher temperatures than the 'amorphous' oxidation products of pyrite decay. The correlation between the temperatures of the final dehydration of crystalline water (Eq. (4)) is, however, consistent for the pyrite specimens, which showed evidence of pyrite disease, indicating the presence of iron(II) sulphate as an oxidation product. This correlates with the observation of sulphate hydrates for significantly oxidised pyrite specimens using X-ray crystallography [1, 3, 4].

Conclusions

This study set out to identify the oxidation products in pyrite specimens which were showing signs of pyrite disease, but whose oxidation products could not easily be identified by other means, such as, crystallography. TG coupled with MS has aided the identification of the oxidation products and confirmed the presence of hydrated iron(II) sulphates. The mechanisms of decomposition of ACS grade iron(II) sulphate in an argon atmosphere has been identified using TG-MS, however, the decomposition mechanisms, of the species produced by pyrite disease, remain uncertain due to the heterogeneity of the oxidised material.

* * *

The authors would like to thank the Australian Museum, Sydney, for the provision of samples and advice in their treatment and characterisation.

References

1 A. Newman, Geo. Curator, 6 (1998) 363.
2 B. J. Reedy, J. K. Beattie and R. T. Lowson, Geochim. Cosmochim. Acta, 35 (1991) 1609.
3 S. L. Borek, ACS Symp. Ser., 550 (1994) 31.

4 S. Chander, R. Zhou and A. Briceno, Min. Met. Proc., 11 (1994) 141.
5 I. I. Maes, J. Yperman, H. van den Rul, D. V. Franco, J. Mullens and L. C. van Poucke, Energy and Fuels, 9 (1995) 950.
6 F. Paulik, J. Paulik and M. Arnold, J. Thermal Anal., 25 (1982) 313.
7 L. Odochian, D. M. Pantea, I. Calugareanu, D. Ionescu and O. Vicol, J. Serb. Chem. Soc., 64 (1999) 737.
8 J. Straszko, M. Olszak-Humienik and J. Mozejko, Inz. Chem. Proc., 17 (1996) 517.